Seismic behaviour of interior reinforced-concrete beam–column sub-assemblages with engineered cementitious composites

Lee, Siong Wee; Tan, Kang Hai; Yang, En-Hua

2018

Lee, S. W., Tan, K. H., & Yang, E.-H. (2018). Seismic behaviour of interior reinforced-concrete beam–column sub-assemblages with engineered cementitious composites. Magazine of Concrete Research, 70(24), 1280-1296. doi:10.1680/jmacr.17.00359

https://hdl.handle.net/10356/89821

https://doi.org/10.1680/jmacr.17.00359

Cite this article
Lee SW, Tan KH and Yang EH (2018)
Seismic behaviour of interior reinforced-concrete beam–column sub-assemblages with engineered cementitious composites.
Magazine of Concrete Research **70(24)**: 1280–1296,
https://doi.org/10.1680/jmacr.17.00359

Research Article
Paper 1700359
Received 10/08/2017; Revised 14/11/2017;
Accepted 23/11/2017;
Published online 22/01/2018

Keywords: cement/cementitious materials/joints/shear

Magazine of Concrete Research

ice publishing

Seismic behaviour of interior reinforced-concrete beam–column sub-assemblages with engineered cementitious composites

Siong Wee Lee
Senior Lecturer, Faculty of Civil Engineering, Universiti Teknologi MARA, Shah Alam, Selangor, Malaysia (corresponding author: slee009@e.ntu.edu.sg)

Kang Hai Tan
Professor, School of Civil and Environmental Engineering, Nanyang Technological University, Singapore

En-Hua Yang
Assistant Professor, School of Civil and Environmental Engineering, Nanyang Technological University, Singapore

The feasibility of using engineered cementitious composites (ECC) in joint cores of reinforced-concrete (RC) beam–column sub-assemblages as a means to enhance seismic behaviour is evaluated. Four RC beam–column sub-assemblages are constructed and tested under lateral cyclic loading. One RC beam–column sub-assemblage with normal concrete in the joint and one RC sub-assemblage with ECC in the joint are designed to gravity loads; neither type has transverse reinforcement in the joint core. Similarly, one RC sub-assemblage with normal concrete in the joint and one with ECC in the joint are designed for seismic provisions, but the latter has no transverse reinforcement in the joint. The test programme thereby allows direct comparison of the structural performance of ECC joints with concrete joints for beam–column sub-assemblages for both gravity and seismic design situations. Results show that the use of ECC joints significantly changes the behaviour of the joint from brittle to ductile. Both ECC specimens exhibit superior damage tolerance, with limited shear distortion and multiple fine cracks in the joints, even though no transverse reinforcement is provided in the joint. Moreover, specimens with ECC joints demonstrate improved bond behaviour in early loading cycles.

Notation

A_c	cross-sectional area of column
A_s	cross-sectional area of tensile reinforcement
b_j	effective width of joint
b_w	width of beam
d	effective depth of beam
f'_c	characteristic compressive strength of concrete
f_{cd}	design compressive strength of concrete
f_{yk}	characteristic yield strength of steel reinforcement
h	storey height of column
h_b	depth of beam
h_c	depth of column
h_i	distance between the top and bottom linear variable differential transducers (LVDTs) at section i
h'_i	distance between the left and right LVDTs at section i
jd	distance between the internal tension and compression force resultants in the beams
l	horizontal distance between beam supports
l'_{b_i}, l'_{c_i}	distance measured from section i to the beam and column end support, respectively
M_b	moments of beam framing into column in the loading direction
M_{Rb}, M_{Rc}	design flexural moments from beams and columns, respectively
N_{Ed}	design axial load of column
s	depth of rectangular stress block
V_c	column shear force
V_j	horizontal joint shear force
v_d	normalised column axial
γ_c	partial factor for concrete
Δ_j	displacement due to shear distortion of the joint
Δ_{bf}, Δ_{cf}	displacement due to flexural deformations of beams and columns, respectively
Δ_1, Δ_2	displacement due to shear distortion of the joint
δ_{iT}, δ_{iB}	reading of LVDTs mounted at the top and bottom faces of beam section i, respectively
δ_{iR}, δ_{iL}	reading of LVDTs mounted at the right and left faces of column section i, respectively
η	reduction factor due to diagonal tension cracking
$\theta_{b,i}$,$\theta_{c,i}$	rotation of beams and column at section i, respectively
v_j	joint shear stress
Υ_j	joint shear distortion

Introduction

When subject to seismic actions, the failure of beam–column joints is one of the main causes that can lead to collapse or major damage of reinforced-concrete (RC) frame structures. In this regard, seismic design provisions emphasise three main aspects in the design of RC beam–column joints, namely, the shear strength of joints, the transverse reinforcement requirement in joints, and the bond behaviour of beam and

column bars passing through the joint cores. Nevertheless, the seismic design of beam–column joints, such as the use of transverse reinforcement in the joint cores, may lead to reinforcement congestion and increase construction difficulties on site. To mitigate congestion in the joints, fibre-reinforced cementitious (FRC) materials may be used, as their effectiveness has been demonstrated in several experimental studies on member behaviour. However, these materials may not be suitable for substituting transverse reinforcement in the joints, because FRC materials exhibit tension-softening behaviour after first cracking and place a limit on shear stress so that premature damage could occur (Parra-Montesinos *et al*., 2005).

In the past two decades, there has been rapid development in engineered cementitious composite (ECC) materials, which are a unique type of high-performance, FRC composite, featuring ultra-high ductility and damage tolerance under direct tensile and shear stresses (Alyousif *et al*., 2015; Li, 2003). Excellent seismic performance can be observed in ECC structural members subject to large inelastic deformations or high shear stress reversals. Previous experimental investigations (Parra-Montesinos and Wight, 2000; Parra-Montesinos *et al*., 2005; Qudah and Maalej, 2014; Said and Razak, 2016; Yuan *et al*., 2013; Zhang *et al*., 2015) have shown the advantageous behaviour of ECC in beam–column joints subjected to cyclic loading. When ECC was used in beam–column joints without any transverse reinforcement, the joints exhibited superior damage tolerance and sustained substantial shear distortions under cyclic loads (Parra-Montesinos, 2005; Parra-Montesinos *et al*., 2005; Said and Razak, 2016; Zhang *et al*., 2015). In the presence of transverse reinforcement, ECC joints significantly increased the load capacity, ductility and energy dissipation (Yuan *et al*., 2013). Compatible deformations between steel reinforcement and ECC were observed at the multiple cracking stage (Fischer and Li, 2002; Kang *et al*., 2015; Li and Fischer, 2002). Moreover, embedded steel reinforcement in ECC could develop significantly higher bond strength than in normal concrete (Hossain *et al*., 2017; Lee *et al*., 2016). Thus, anchorage bond failure could be avoided in the joints due to the enhanced bond strength of the embedded steel reinforcement in the ECC.

Although the advantages of using ECC in beam–column joints have been reported through previous research studies (Parra-Montesinos and Wight, 2000; Parra-Montesinos *et al*., 2005; Qudah and Maalej, 2014; Said and Razak, 2016; Yuan *et al*., 2013; Zhang *et al*., 2015), there are still some technical gaps in understanding. First, previous research incorporated ECC material in the joint cores and throughout the plastic hinge lengths of beams and columns (Parra-Montesinos *et al*., 2005; Qudah and Maalej, 2014; Said and Razak, 2016; Yuan *et al*., 2013; Zhang *et al*., 2015). In this study, ECC material (without any transverse reinforcement) was only incorporated in the joint cores for the two sub-assemblages consisting of RC beams and columns. This is because ECC material costs about four times more than normal concrete and thus its use should be kept to a minimum. Second, the behaviour of the bond between reinforcement and ECC was not addressed in some of the tests (Qudah and Maalej, 2014; Said and Razak, 2016), yet bond strength is particularly important for evaluating the enhancement in bond–slip behaviour of beam longitudinal bars passing through the joints. Third, some studies did not address the shear strength (Said and Razak, 2016; Yuan *et al*., 2013) of beam–column joints made with ECC. This made the assessment of the shear strength of ECC joints challenging, and comparison of the test results with code-defined limiting shear strength values could not be carried out. Finally, there are hardly any publications addressing the seismic design of beam–column sub-assemblages (made of ECC or normal concrete joints) based on Eurocode 8 (BSI, 2004a). It should be mentioned that comparison of test results with Eurocode 8 (BSI, 2004a) was not made in any of the works described above (Parra-Montesinos and Wight, 2000; Parra-Montesinos *et al*., 2005; Qudah and Maalej, 2014; Said and Razak, 2016; Yuan *et al*., 2013; Zhang *et al*., 2015). To address the aforementioned limitations in the existing literature, the present study was carried out to gain a deeper knowledge of the behaviour of beam–column joints made of ECC when subjected to cyclic loading.

This paper presents an experimental investigation of the behaviour of four internal beam–column cruciform sub-assemblages subject to horizontal cyclic loads at the column top. Seismic design and detailing of the beam–column sub-assemblages were in accordance with Eurocode 8 (BSI, 2004a). Comparisons of the hysteretic response, failure mode, analysis of inter-storey drift contribution, distribution of beam and column longitudinal bar strains, joint shear stress and energy dissipation were made between sub-assemblages with joint cores either made of ECC or conventional concrete material.

Experimental programme

Specimen design

Beam–column sub-assemblages were extracted from a prototype six-storey office building with a typical height of 3·6 m. The centre-to-centre spacing of columns in two orthogonal directions was 5·4 m. The dimensions of beams and columns were 300 mm wide by 500 mm deep and 500 mm wide by 500 mm deep, respectively. The specimens were scaled down to a one-half model, as shown in Figure 1. Table 1 shows the details of the four beam–column sub-assemblages. In the notation, CIJ denotes concrete interior joint; EIJ represents ECC interior joint (or joints made of ECC without transverse reinforcement); S and NS refer to seismic and non-seismic (gravity) design, respectively; and numerals 1 and 0 indicate joints with and without joint transverse reinforcement, respectively. Two types of design were adopted in this study. Two specimens, namely, CIJ-NS-0 and EIJ-NS-0, were designed for gravity loads in accordance with Eurocode 2 (BSI, 2004b); the

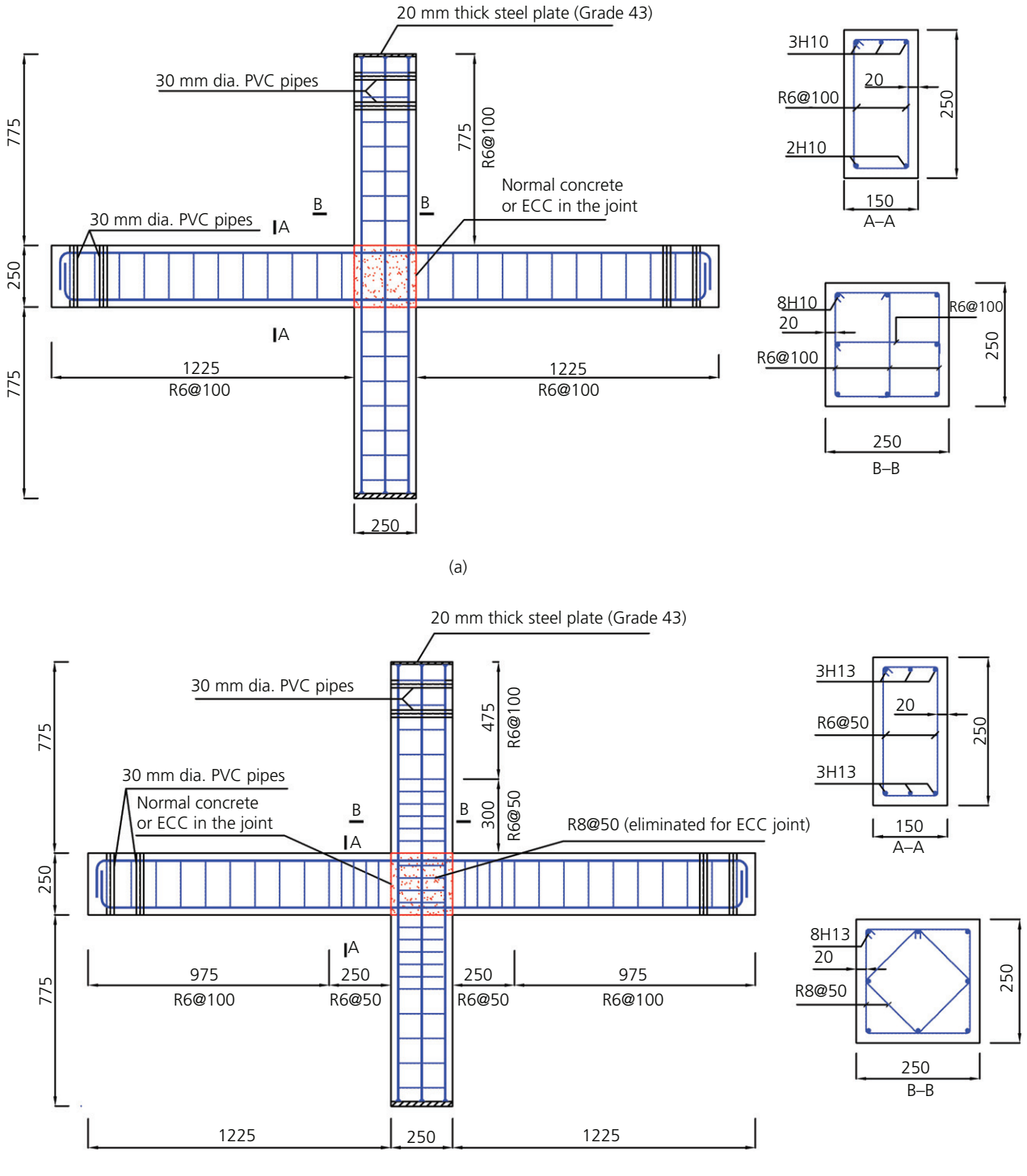

Figure 1. Detailing of beam–column sub-assemblages: (a) CIJ-NS-0 and EIJ-NS-0 (non-seismic design to Eurocode 2); (b) CIJ-S-1 and EIJ-S-0 (seismic design to Eurocode 8) (units in mm)

other two specimens, namely, CIJ-S-1 and EIJ-S-0, were designed according to seismic ductility class DCM (medium ductility), as specified in Eurocode 8 (BSI, 2004a). However, it is worth mentioning that the strong-column–weak-beam design concept was not strictly compliant with Eurocode 8, in which the column flexural strength to beam flexural strength ratio ($\Sigma M_{Rc}/\Sigma M_{Rb}$) is less than 1·30. Generally, both sets of specimens had the same longitudinal reinforcement in beams and

Table 1. Details of specimens

Specimen	Material in joint core	Type of design	Joint transverse reinforcement (ratio: %)	Longitudinal bars in beam	Longitudinal bars in column
CIJ-NS-0	Concrete	Non-seismic	0	3H10 (top)	8H10
EIJ-NS-0	ECC	Non-seismic	0	2H10 (bottom)	
CIJ-S-1	Concrete	Seismic	4R8@50 (0·8%)	3H13 (top)	8H13
EIJ-S-0	ECC	Seismic	0	3H13 (bottom)	

Note: H13 and H10 denote high-yield-strength deformed reinforcement with nominal diameters of 13 mm and 10 mm, respectively. R8 denotes low-yield strength mild steel bar with nominal diameter of 8 mm. The concrete clear cover is 20 mm, measured from the beam surface to the outermost edge of the stirrups

columns under either Eurocode 2 (CIJ-NS-0 and EIJ-NS-0 for gravity design) or Eurocode 8 (CIJ-S-1 and EIJ-S-0 for seismic design) as shown in Figure 1 and Table 1.

In specimens with non-seismic design (CIJ-NS-0 and EIJ-NS-0), joint transverse reinforcement was not provided and normal concrete and ECC were used in the joint cores, respectively. In CIJ-S-1 with seismic design, joint transverse reinforcement was provided in the joint core made of normal concrete, whereas only ECC was used in the joint core of EIJ-S-0 so that the effectiveness of the ECC (without joint transverse reinforcement) in resisting shear force could be assessed. Thus, specimen EIJ-S-0 satisfied the seismic design requirements of Eurocode 8 for longitudinal reinforcement in beams and columns, but not the provision of transverse reinforcement in the joint. Two stages of casting were adopted for the specimens with ECC in the joint (EIJ-NS-0 and EIJ-S-0). Concrete beams and columns were cast initially in the first stage. The ECC mix was then poured into the joint cores during the second stage. Thus, four cold joints were formed at the beam–column joint interfaces of the EIJ specimens. It is worth noting that all of the cold joint interfaces were intentionally roughened before placement of the ECC to ensure adequate interface shear strength between the structural members and the joint core. For CIJ-NS-0 and CIJ-S-1 sub-assemblages, casting was done in a single stage and there were no cold joints.

Test set-up and instrumentation

Figure 2 shows the test set-up for beam–column sub-assemblages. The column was connected to the testing floor through a pin support. Both ends of the beam were restrained against vertical displacements by two load cells, by means of which the vertical reaction forces could be measured. A horizontal load was applied to the column top. Figure 3 shows the loading scheme. It ranged from the minimum drift ratio of 0·5% (equivalent to 9 mm horizontal displacement) to the maximum of 6·0% (108 mm displacement), or an even higher drift ratio until the specimen failed to resist the applied load. Although Eurocode 8 only specifies the maximum inter-storey drift ratio up to 2·0% for RC tall building structures, more loading cycles have been applied beyond this limit to evaluate seismic performance of the four beam–column sub-assemblages up to failure. The drift ratio is defined as the inter-storey displacement divided by the column height. Two loading cycles were repeated in each drift ratio to evaluate the loss of strength and stiffness of the joint. In this test, no axial load was applied to the column to consider the most critical scenario under seismic loading conditions, as previous studies have demonstrated that a moderate or high axial load actually improved the shear strength of the joint (Priestley and MacRae, 1996).

Figure 4 shows the layout of the linear variable differential transducers (LVDTs) and strain gauges. LVDTs were mounted in the plastic hinge regions of the beams and columns to measure member flexural deformations. In addition, two diagonal LVDTs were installed in the joint core to measure relative shear distortions, as shown in Figure 4(a). Strain gauges were mounted on longitudinal reinforcement in the beams and columns, and transverse reinforcement in the joint (Figure 4(b)), so that the stress state of the longitudinal bars and transverse reinforcement in the joint could be monitored. TML strain gauges with 5 mm gauge length and 10 m length of lead wire were bonded to steel reinforcement using cyanoacrylate (CN) adhesives.

Material properties

High-strength deformed bars H10 and H13 were used for longitudinal reinforcement in columns and beams, whereas mild steel bars R8 and R6 were used as shear links in columns and beams. It should be noted that, although Eurocode 8 no longer accepts mild steel bars, owing to the scaled-down dimensions of the sub-assemblages, mild steel bars can be easily placed inside the formwork because of the reduced internal radius of bend. Table 2 summarises the material properties of the steel reinforcement and concrete. Each value was obtained from three samples for every size of reinforcement and the same batch of concrete. Figure 5 shows typical stress–strain curves of longitudinal reinforcement H10 and H13. It is worth noting that the material properties of ECC play an important role in the joint behaviour under seismic action. In this study, the ECC was tailor made using locally available ingredients, in which Portland cement, ground granulated blast-furnace slag (GGBS), silica sand, water, superplasticiser and polyvinyl alcohol (PVA) fibres were mixed thoroughly before casting.

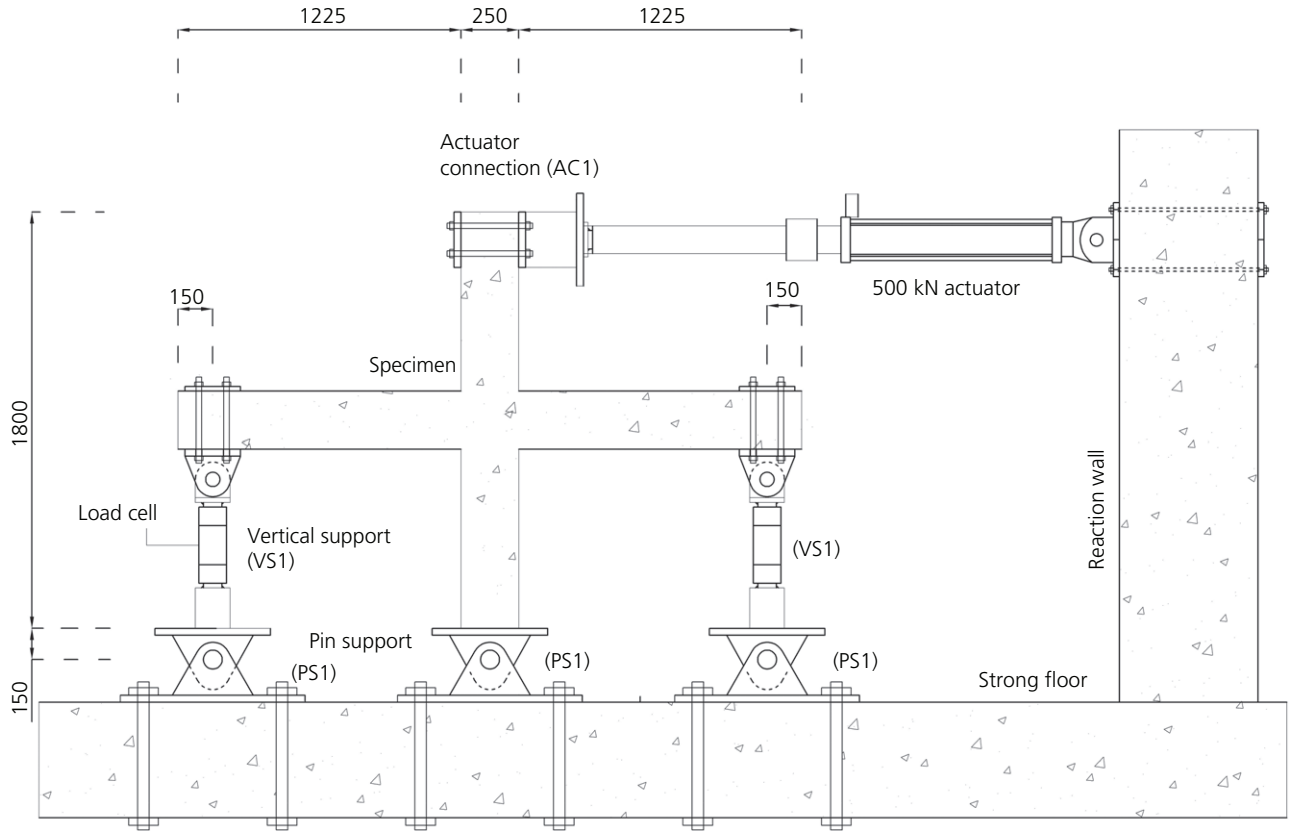

Figure 2. Test set-up (dimensions in mm)

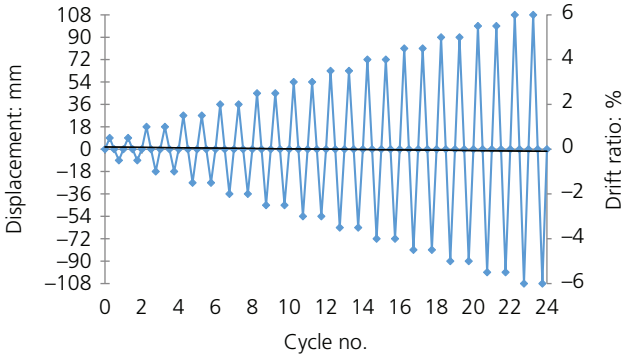

Figure 3. Loading history

Table 3 shows the mix design of the ECC in which the water–binder ratio was 0·27 and 60% of the binder was GGBS. The volume fraction of PVA fibres with 39 μm dia. and 12 mm length was 2%. The material properties of the ECC were obtained by means of compression and uniaxial tension tests. The average compressive strength of three 50 mm (diameter) by 100 mm (height) cylinders was 50·3 MPa. When subject to uniaxial tension, ECC dog-bone specimens with a cross-section of 10·5 mm (thickness) by 35·5 mm (width) and a gauge length of 125 mm exhibited moderate tensile strain-hardening behaviour, as shown in Figure 6. The first cracking strength of ECC was 3·2 MPa. Thereafter, multiple cracks developed along the gauge length, leading to several drops of applied load prior to failure. The average tensile strength and strain capacity of ECC coupons was around 3·4 MPa and 1·0%, respectively.

Test results and discussion

The flexural strength ratio ($\Sigma M_{Rc}/\Sigma M_{Rb}$), which represents the column flexural strength to beam flexural strength ratio, was calculated from actual material properties of the concrete and steel reinforcement. The formula for estimating flexural strength (M_{Rb} or M_{RC}) is given as

1. $$M_{Rb} = 0{\cdot}87 f_{yk} A_s (d - s/2)$$

where f_{yk} is the characteristic yield strength of the steel reinforcement; A_s is the cross-sectional area of the tensile reinforcement; d is the effective depth of the beam; and s is the depth of the rectangular stress block ($s = (0{\cdot}87 f_{yk} A_s / 0{\cdot}567 f'_c b_w)$), in which f'_c is the characteristic compressive strength of concrete and b_w is the width of the beam. The calculated flexural strength ratio for all specimens was 1·03, which was below the

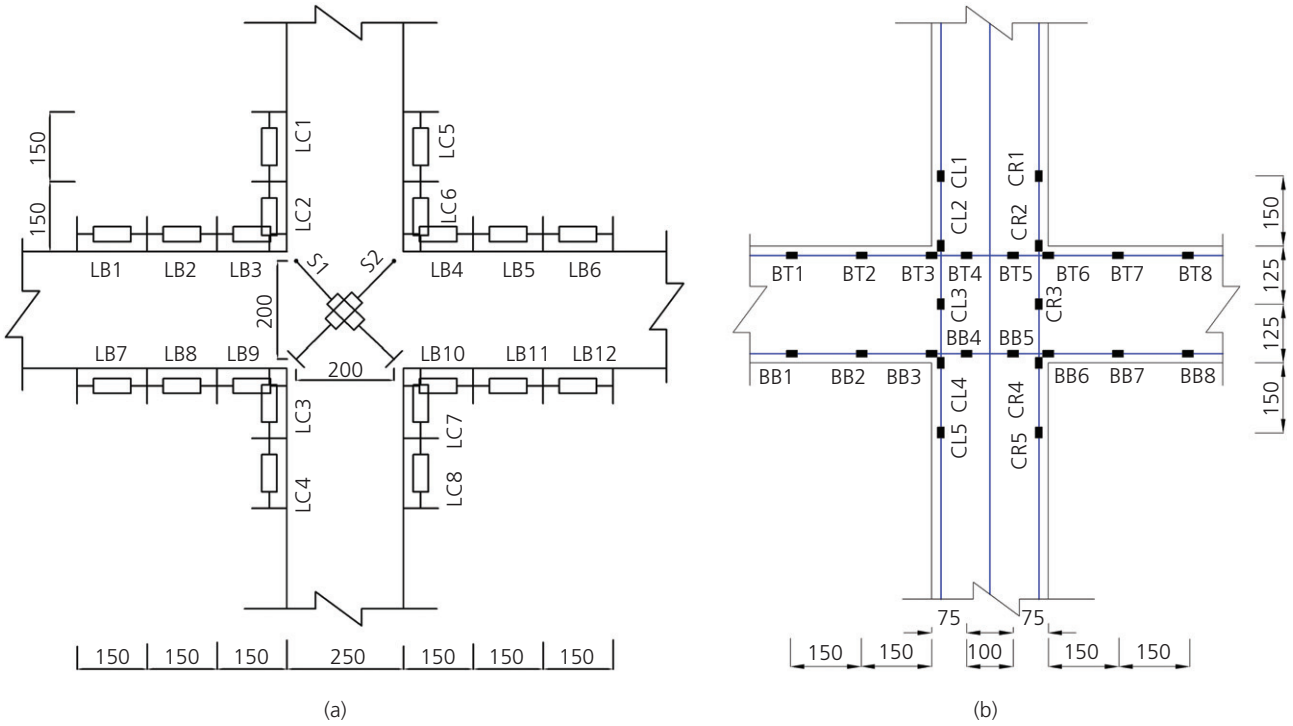

Figure 4. Instrumentation: (a) layout of LVDTs; (b) layout of strain gauges

Table 2. Material properties of reinforcing bars and concrete

Material	Bar type	Bar diameter: mm	Yield strength: MPa	Elastic modulus: GPa	Ultimate strength: MPa	Fracture strain: %
Longitudinal bar H13	High strength	13	540	216·0	644	10·5
Longitudinal bar H10	High strength	10	515	190·7	609	7·8
Stirrups R8	Mild steel	8	250	199·5	348	52·5
Stirrups R6	Mild steel	6	225	195·0	358	35·1
	Compressive strength: MPa		**Splitting tensile strength: MPa**		**Modulus of elasticity: GPa**	
Concrete	24·7		2·8		23·3	

Note: R6 denotes low-yield-strength mild steel bar with nominal diameter of 6 mm

minimum flexural strength ratio of 1·30 as requested by Eurocode 8. The concept of strong-column–weak-beam was not strictly adhered to in this series of tests, to avoid failure in the beams and to facilitate failure in the joints made of normal concrete. This was to allow the assessment of ECC against normal concrete in the joint cores.

By applying a reversible horizontal load to the column top, the behaviours of beam–column sub-assemblages were observed, and these are summarised in Table 4. The maximum load and failure load were taken in the positive loading direction (push). All the tests were terminated after the full cycle of that particular drift ratio when the residual load resistance of the specimen dropped to 85% of its maximum load capacity (Li *et al.*, 2015; Yuan *et al.*, 2013).

Hysteretic response and failure mode

Figures 7 and 8 show the hysteresis loops of the four beam–column sub-assemblages. As for control specimen CIJ-NS-0 with non-seismic design, a few flexural cracks on the beams were initiated at a drift ratio of 1·0%. With increasing horizontal displacement at the column top, more cracks were formed along the entire beam length, propagating from the beam top or bottom surfaces depending on the loading direction. The maximum horizontal load of 26·18 kN was attained at a drift ratio of 3·5%. Crushing of concrete was observed in the compression zones of the beams at a drift ratio of 5·0%. Subsequently, spalling of concrete occurred at the left joint interface, as well as in the left column region above the joint (Figure 7(a)) due to extension of joint diagonal cracks during a drift ratio of 6·0%. Final failure was caused by widening

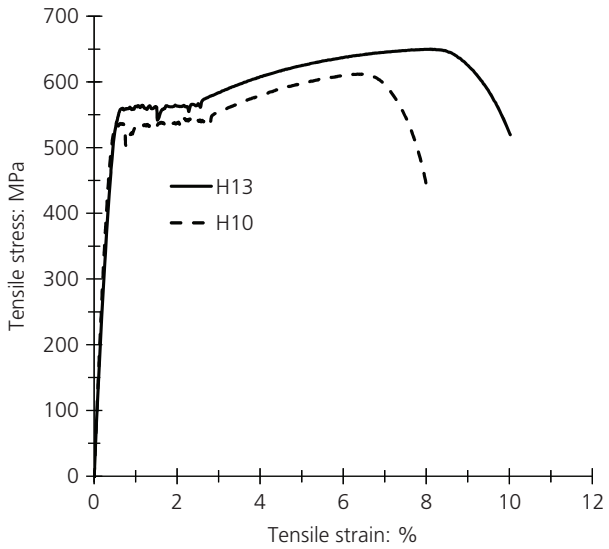

Figure 5. Stress–strain curve of reinforcing bars

of diagonal shear cracks within the joint core (Figure 7(a)). This mode of failure is typical for beam–column joints without transverse reinforcement. In particular, when the applied joint shear stress was large, significant diagonal tensile cracks in both diagonal directions occurred (Hakuto *et al.*, 2000).

When ECC was used in the joint core, beam–column joint EIJ-NS-0 had different behaviour from that of control specimen CIJ-NS-0 (see Figure 7(b)). It achieved the maximum load capacity of 23·82 kN at 3·0% drift ratio. Thereafter, a sudden drop of load took place during the second cycle of 4·0% drift ratio due to fracture of the beam top reinforcement at the right joint interface. Subsequently, the horizontal load decreased to 18·42 kN at 4·5% drift ratio. Although the maximum loads in the following cycles were less than 85% of the load capacity, testing was continued to the maximum drift ratio of 6·0% for the purpose of comparison. The hysteretic response in the negative loading phase exhibited good ductility up to a drift ratio of 6·0%. During the second cycle of negative loading at a drift ratio of 6·0%, fracture of the beam top reinforcement was observed at the left joint interface, leading to significant pinching of the hysteretic curve, as shown in Figure 7(b). However, no major damage was observed in the joint core. The fracture of the beam top longitudinal bars at both joint interfaces was caused by widening of cracks at the joint interfaces because of the different materials in the beams and the joint core.

Specimen CIJ-S-1 with seismic design and detailing developed a load capacity of 40·98 kN at a drift ratio of 3·5%, as shown in Figure 8(a). In addition to flexural cracks in the beams and the column, visible diagonal shear cracks were formed in the joint core. As a result, severe pinching could be found in the hysteretic curve of the joint. During the second cycle of 5·0% drift ratio, crushing of concrete occurred in the joint core. With increasing horizontal displacement at the column top, spalling of concrete in the joint core was observed. Eventually, the specimen failed by diagonal crushing of compressive struts in the joint core at 6·5% drift ratio.

As for specimen EIJ-S-0, even though there was no joint transverse reinforcement, its behaviour was substantially improved by using ECC in the joint core. Compared to CIJ-S-1, its maximum load capacity was approximately 15% greater. The peak load of 47·38 kN was attained at a drift ratio of 4·0% compared to 3·5% for CIJ-S-1. Brittle joint failure was prevented in EIJ-S-0. Again, crushing and spalling of the concrete occurred at the beam ends adjacent to the joint, as shown in Figure 8(b). In the joint core, multiple fine cracks were observed with limited crack widths at the final stage, due to improved ductility of the ECC in comparison with normal concrete.

Both specimens with ECC in the joint core (EIJ-NS-0 and EIJ-S-0) showed beam end failure mode near the joint, as observed in Figures 7(b) and 8(b), despite the flexural strength ratio ($\Sigma M_{Rc}/\Sigma M_{Rb}$) being below 1·30 as specified in Eurocode 8. Therefore, the strong-column–weak-beam requirement in the design of beam–column interior joints could be somewhat relaxed if ECC were to be used in the joint cores. For the concrete specimens (CIJ-NS-0 and CIJ-S-1), brittle joint failures were observed in Figures 7(a) and 8(a) as the beams were designed to have comparable flexural strength with that of the column. As ECC materials possess good damage tolerance and multiple-cracking behaviour, shear failure in the joints can be prevented. Prevention of shear failure in the joints was also demonstrated in Parra-Montesinos' test (Parra-Montesinos *et al.*, 2005), despite the total substitution of the joint transverse reinforcement with high-performance fibre-reinforced concrete composite in the joint core and adjacent beam plastic regions.

Analysis of inter-storey drift contributions

Total horizontal displacement at the column top was mainly contributed by several major components, namely, flexural deformations of the beams and columns, and shear distortions of the joints. Contributions of the aforementioned components

Table 3. Mix proportions of ECC

Ingredient	Cement	GGBS	Water	Silica sand	Superplasticiser	PVA fibre
Unit weight: kg/m^3	574	860	387	287	3–3·5	26

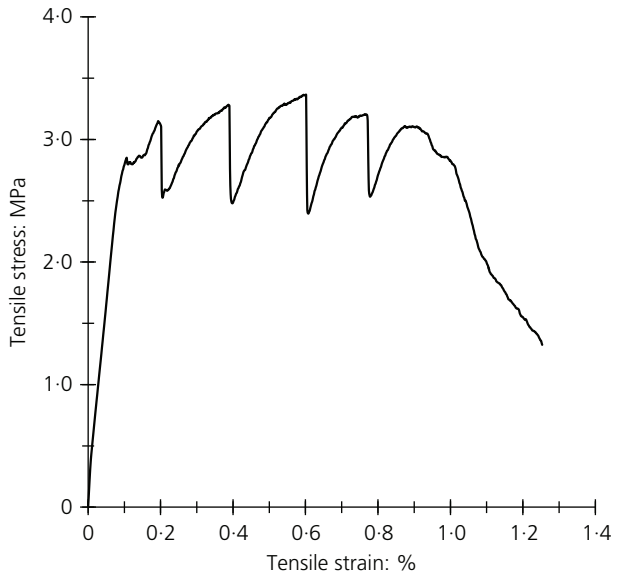

Figure 6. Tensile test of ECC

could be calculated from the measured deformations by LVDTs (see Figure 4(a)) based on the method and procedure employed in previous research (Hakuto, 1995). The beam and column shear deformations were neglected, as they were assumed to be small compared with the three major components (Ashtiani *et al.*, 2014). The method of calculating displacements due to flexural deformations of beams and columns, and shear distortions of joints, is given in the Appendix. It is worth noting that the total sum of the components of deformations did not add up to the recorded imposed drift as shown in Figure 9. This could be due to the assumptions in the method. During larger drift ratio – that is, 3·0% onwards – shear deformations and inelastic deformations in beams and columns accumulated; also the flexural deformations of beams outside the plastic hinge regions were not accounted for in the model shown in the Appendix. The errors in the estimation of the percentage contribution to drift seem larger during smaller drift ratio, possibly due to the lack of sensitivity of the instrumentation when the applied loads were small. For CIJ-S-1, the total contribution during a drift ratio of 6·0% was more than 100%, in which joint shear distortion contributed significantly compared to the previous loading cycles. This implied that major diagonal cracks had occurred in CIJ-S-1, and the crack openings could not be closed under load reversal during the last drift ratio.

The relative percentage contributions of flexural deformations of beams, flexural deformations of the column and shear distortion of the joint were calculated with respect to their sum (Ashtiani *et al.*, 2014). Figure 10 shows the relative contributions of the three components to total drift. In all of the four specimens, shear distortion of the joint contributed little to total drift prior to diagonal cracking. Total drift was mainly caused by flexural deformations of beams for all specimens except CIJ-S-1 during a drift ratio of 6·0%. Only CIJ-S-1 experienced severe joint damage as a result of crushing of diagonal struts and spalling of concrete in the joint. Thus, it can be seen that 40% of total drift resulted from the joint distortion during the drift ratio of 6·0%, whereas flexural deformations of the beams and the column were smaller (Figure 10(c)). However, for ECC specimens (EIJ-NS-0 and EIJ-S-0), flexural deformations of beams contributed more than 50% of total drift throughout the loading cycles. This agreed well with the observed beam flexural failure mode, as shown in Figures 7(b) and 8(b). Likewise, the contribution of joint shear distortion was reduced significantly (85–90%) by using ECC in the joint core. Generally, column flexural deformations were less significant than beam flexural deformations for all cases (see Figure 9) due to greater flexural rigidities of the columns than the beams, as well as yielding of the beam longitudinal bars. Analysis of inter-storey drift contributions confirmed that ECC considerably changed the brittle joint failure to beam flexural failure as discussed in the earlier section entitled 'Hysteretic response and failure mode'.

Strain distribution along beam longitudinal bars

Figure 11 shows the measured strain profile along the top longitudinal bars in the beam. In CIJ-NS-0, the beam top reinforcement at the left joint interface was in tension (Figure 11(a)) owing to a relatively low ratio of tensile reinforcement at the bottom and limited neutral axis depth at the top. With

Table 4. Summary of the test results

Specimen	Flexural strength ratio, $\frac{\Sigma M_{Rc}}{\Sigma M_{Rb}}$	Maximum load: kN	Failure load: kN	Drift ratio: %		Final failure mode
				Maximum load	Failure load	
CIJ-NS-0	1·03	26·18	21·00	3·5	6·0	Diagonal shear cracks in the joint core and crushing of concrete at column region above joint
EIJ-NS-0	1·03	23·82	18·42	3·0	4·5	Fracture of rebar and crushing of concrete at beam ends adjacent to the joint. No internal joint failure
CIJ-S-1	1·03	40·98	33·10	3·5	6·5	Diagonal crushing of concrete at joint core
EIJ-S-0	1·03	47·38	38·24	4·0	6·5	Crushing of concrete at beam ends adjacent to the joint. No internal joint failure

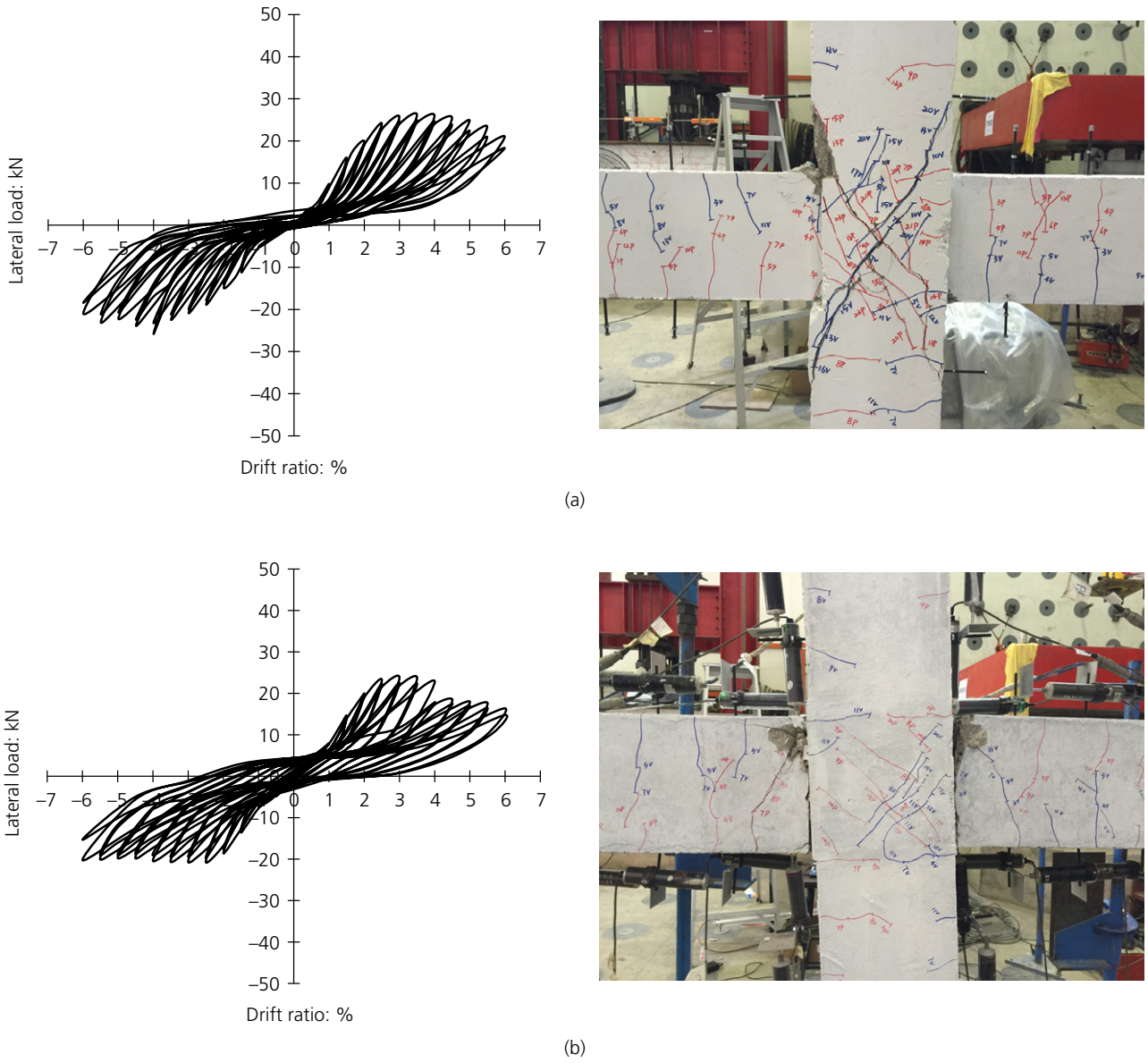

Figure 7. Load–displacement hysteresis loops and final failure modes for non-seismic design specimens: (a) CIJ-NS-0 (control specimen); (b) EIJ-NS-0

increasing drift ratio, tensile strains started developing at the beam top bars. However, for EIJ-NS-0, compression stresses were generated at the left joint interface of the beam top reinforcement (Figure 11(b)) prior to a drift ratio of 2·0%. Compared with CIJ-NS-0, the anchorage bond strength was improved in EIJ-NS-0 based on a greater gradient of strain profile along the anchorage length before a drift ratio of 4·0%. Strain readings could not be obtained at the right beam–column joint interface at a drift ratio of 4·0% and beyond, as fracture of rebar had already occurred by then.

Figure 11(c) shows the distribution of strain along the beam top longitudinal bars for CIJ-S-1. Generally, strains in the beam bars were kept below the yield strain. The beam top bar was just about to yield at the left joint interface during the final loading stage, as shown in Figure 11(c). Without yielding of the top bars, the beam flexural strength was unable to develop and instead joint shear failure occurred. For EIJ-S-0, the beam bars in the tension zone yielded after a drift ratio of 3·0% (Figure 11(d)), indicating the development of beam flexural strength, which contributed to greater lateral load capacity. According to Tsonos (2007), the ability of members to develop their flexural strength before failing in shear is of great interest in the seismic design of beam–column joints. A greater gradient of the strain profile along the anchorage length in this specimen implied that ECC has improved the

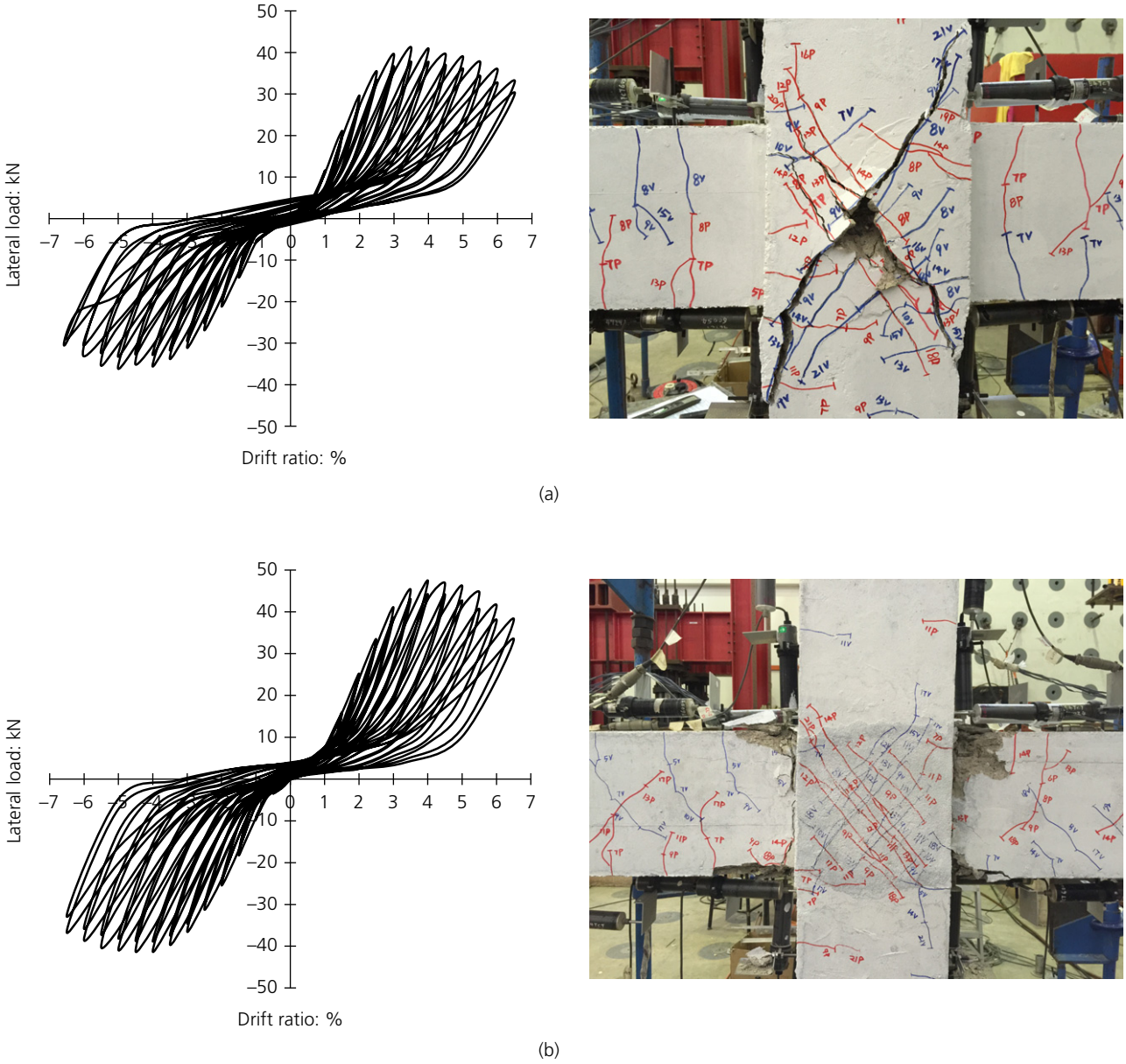

Figure 8. Load–displacement hysteresis loops and final failure modes for seismic design specimens: (a) CIJ-S-1 (control specimen); (b) EIJ-S-0

bond strength up to a drift ratio of 3·0% compared with specimen CIJ-S-1.

In the ECC specimens, larger strain values at the left and right joint interfaces were obtained (Figures 11(b) and 11(d)), possibly due to widening of cracks at the vertical cold joint interfaces as the drift ratio increased. Consequently, concrete crushing at the beam ends occurred and led to beam flexural failure of the ECC specimens. Figure 12 shows the strain history of the joint transverse reinforcement for CIJ-S-1. Positive strain readings at the joint transverse reinforcement for CIJ-S-1 indicated that the transverse reinforcement had yielded at a drift ratio of about 4·0%, as shown in Figure 12. Strain profiles at A, B, C and D were rather symmetrical about the centre of the joint core in CIJ-S-1, indicating a good symmetric test set-up. Unfortunately, strain readings after the drift ratio of 4·0% could not be recorded. In subsequent loading cycles, the efficiency of the joint transverse reinforcement in transmitting shear forces was reduced, leading to compressive strut failure of the joint in CIJ-S-1.

Strain distribution along column longitudinal bars

Figure 13 shows the typical strain profile of the column longitudinal reinforcement passing through a joint made of either

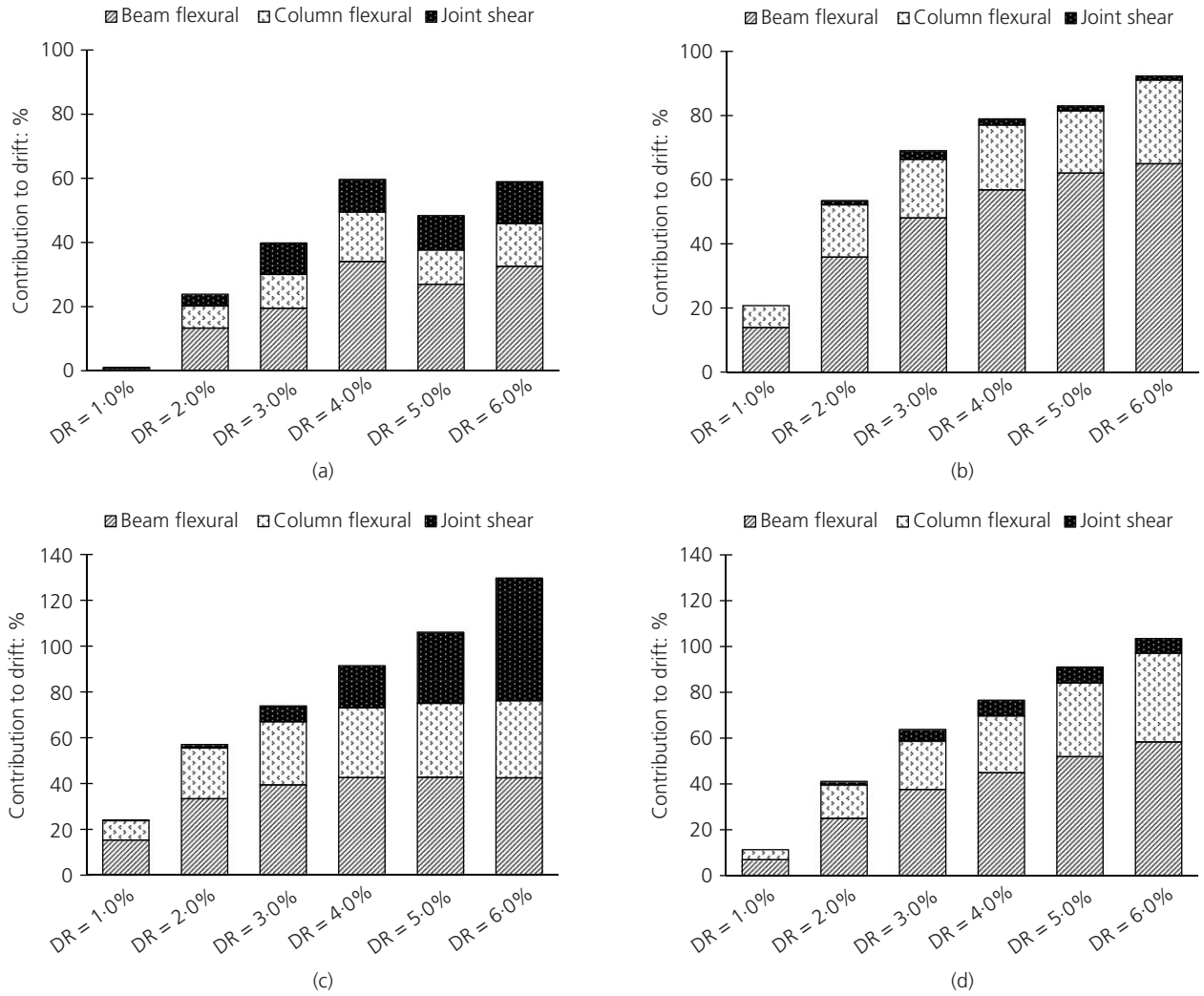

Figure 9. Contributions to the overall imposed drift: (a) CIJ-NS-0; (b) EIJ-NS-0; (c) CIJ-S-1; (d) EIJ-S-0 (DR, drift ratio)

concrete or ECC. For the concrete specimen (CIJ-NS-0), the column longitudinal reinforcement did not yield at failure. Owing to the presence of cold joints in the ECC specimen (EIJ-NS-0), the column reinforcement yielded at the bottom joint interface at a drift ratio of 3·0%. Away from the joint interface, the column reinforcement was in the elastic stage. Despite the yielding of the column reinforcement, the ECC specimens demonstrated better bonding than the concrete specimens. This can be seen from the greater slope gradient exhibited by the strain profile across the beam depth, as shown in Figure 13(b).

Joint shear stress

Horizontal shear force at the mid-depth of the joint core can be calculated based on the following formula (Parra-Montesinos *et al.*, 2005)

$$V_j = \sum \frac{M_b}{jd} - V_c \quad (2)$$

where M_b is the moment of the beam framing into the column in the loading direction; jd is the distance between the internal tension and compression force resultants in the beams (taken as $0{\cdot}9d$); and V_c is the column shear force. Furthermore, joint shear stress (v_j) can be estimated as:

$$v_j = \frac{V_j}{b_j h_c} \quad (3)$$

where b_j is the effective joint width and h_c is the column depth. The calculated maximum joint shear stress was compared with the allowable joint shear stress specified by Eurocode 8 (BSI, 2004a), New Zealand standard NZS 3101 (SNZ, 2006) and ACI standard ACI 318-14 (ACI, 2015), so that a comparison could be made between these three design codes. This kind of comparison study has rarely been reported in previous research studies. According to NZS 3101, the joint shear stress limit is $0{\cdot}20f'_c$ or 10 MPa (whichever is smaller), whereas it is 1·25

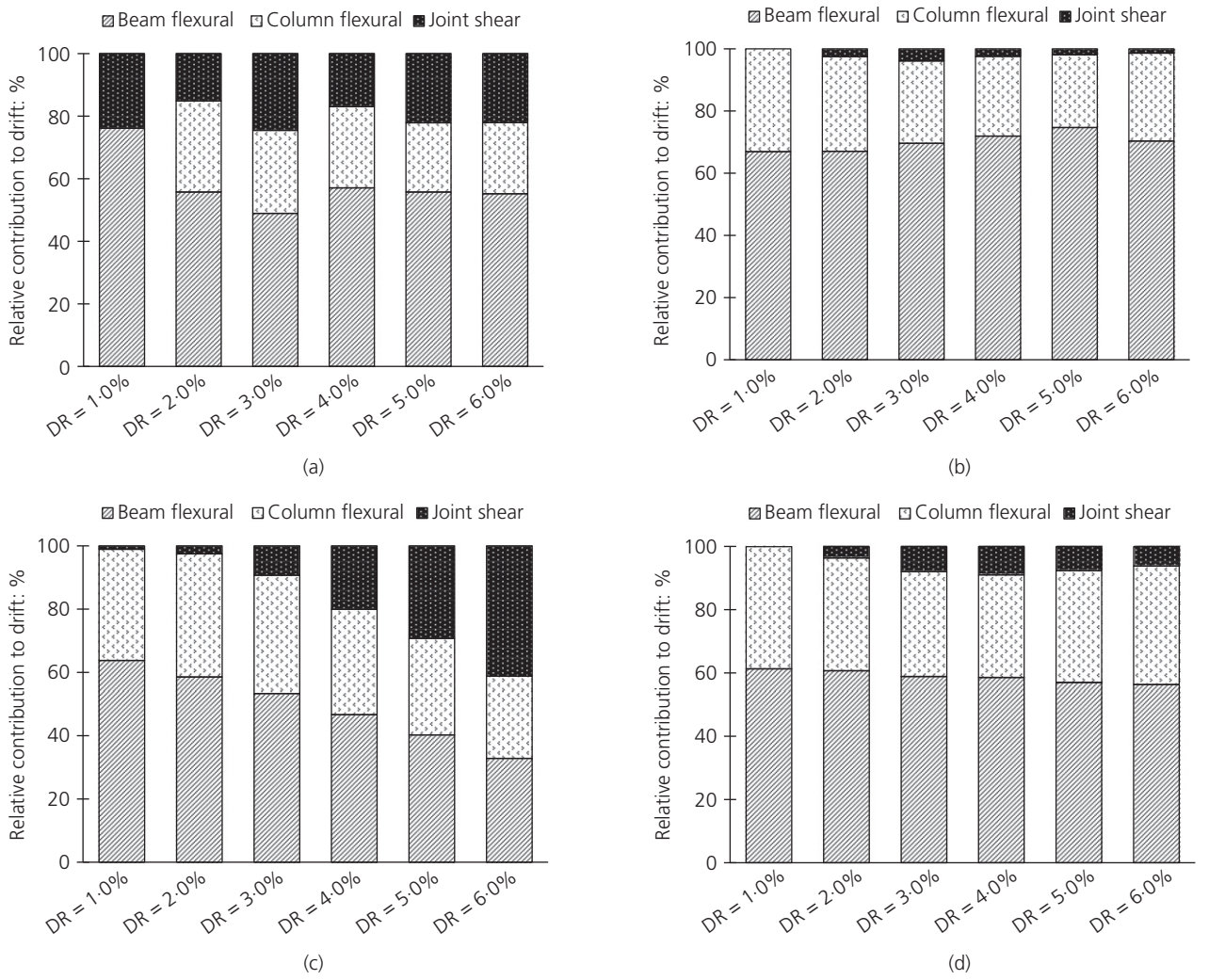

Figure 10. Relative contributions to the total calculated drift: (a) CIJ-NS-0; (b) EIJ-NS-0; (c) CIJ-S-1; (d) EIJ-S-0 (DR, drift ratio)

$\sqrt{f'_c}$ according to ACI 318-14. However, Eurocode 8 specifies the permitted beam–column joint shear stress as

4. $$v_{\text{jlimit}} \leq \eta f_{\text{cd}} \sqrt{1 - \frac{v_{\text{d}}}{\eta}}$$

5. $$\eta = 0{\cdot}6\left(1 - \frac{f'_{\text{c}}}{250}\right)$$

6. $$f_{\text{cd}} = \frac{f'_{\text{c}}}{\gamma_{\text{c}}}$$

7. $$v_{\text{d}} = \frac{N_{\text{Ed}}}{A_{\text{c}} f_{\text{cd}}}$$

where η is the reduction factor due to diagonal tension cracking; f'_c is the characteristic compressive strength of concrete; f_{cd} is the design concrete strength; γ_c is the partial factor for concrete (taken as 1·5 by assuming persistent and transient design situations); v_d is the normalised column axial load ratio; N_{Ed} is the design axial load of the column; and A_c is the cross-sectional area of the column. It is worth mentioning that the effective width of the joint as defined in Equation 3 was determined according to the respective code. According to Eurocode 8, NZS 3101 and ACI 318-14, the effective width of the joint is taken as 250 mm (Figure 1). Notable in Eurocode 8, h_c is taken as the distance between extreme layers of column reinforcement (i.e. 200 mm), whereas h_c is taken as 250 mm based on NZS 3101 and ACI 318-14. Therefore, the calculated shear stress was identical according to NZS 3101 and ACI 318-14 due to the same effective area of the joint core. Table 5 shows the ratio of maximum joint shear stress from tests to limiting joint shear stress by the three different codes (ratio v_{j_max}/v_{jlimit}).

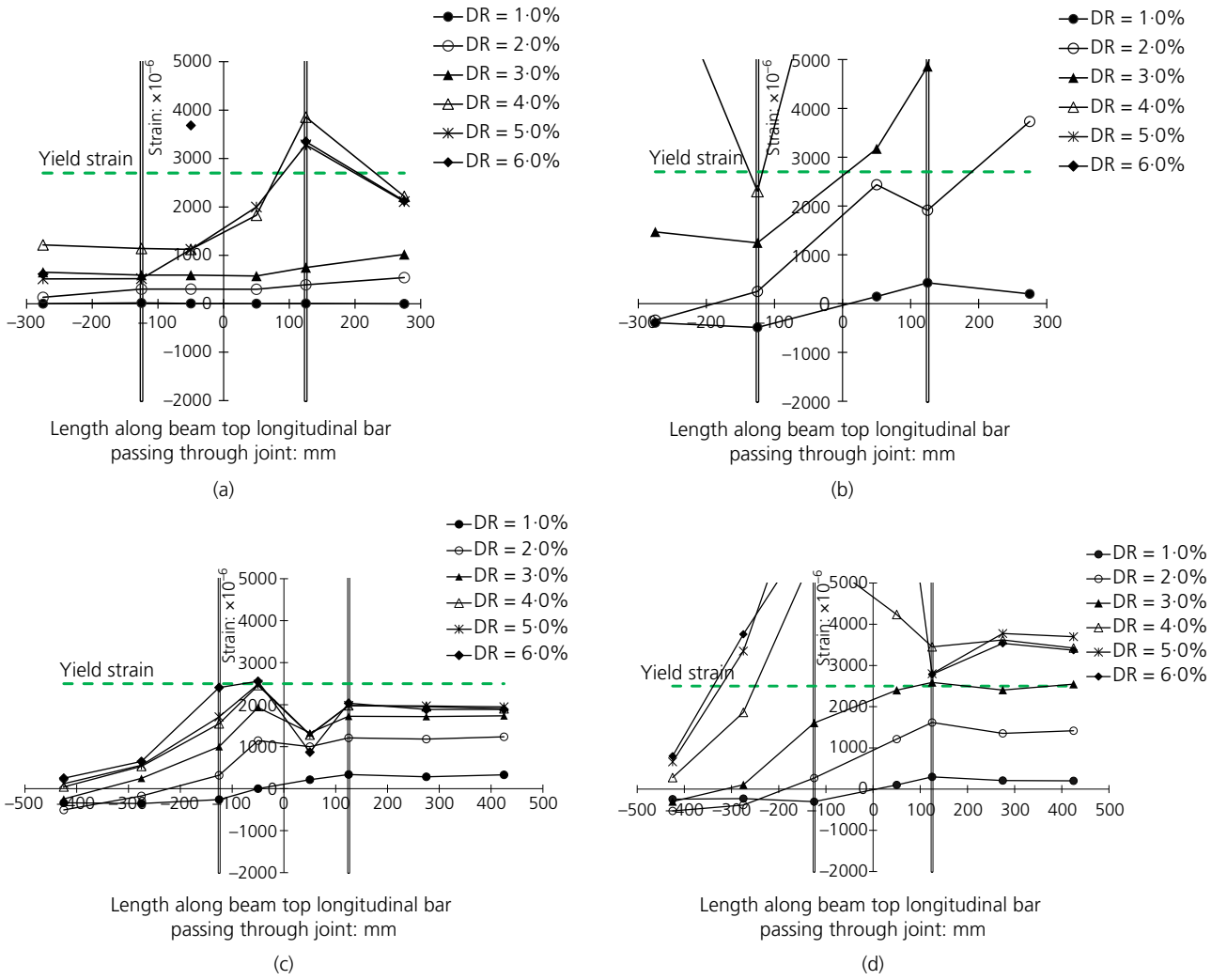

Figure 11. Distribution of strain along beam top longitudinal bars passing through the joint core: (a) CIJ-NS-0; (b) EIJ-NS-0; (c) CIJ-S-1; (d) EIJ-S-0 (DR, drift ratio)

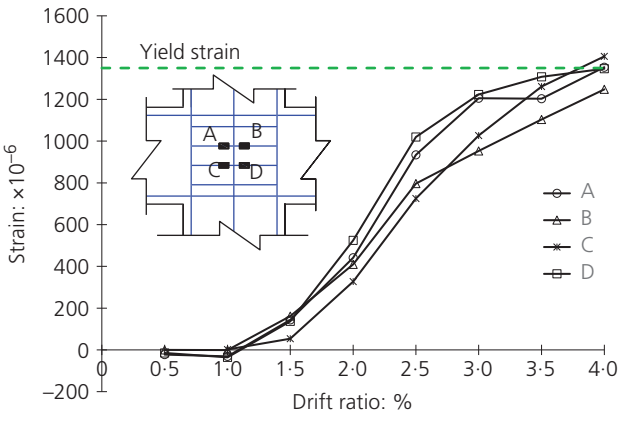

Figure 12. Strain history of joint transverse reinforcement for CIJ-S-1

For non-seismic design specimens (CIJ-NS-0 and EIJ-NS-0), the maximum joint shear stresses were well below the limits specified by the three codes as diagonal compression shear failure was not observed in any of the joints. The maximum shear stress of joint CIJ-S-1 exceeded the allowable shear stress limit specified in NZS 3101, as crushing of diagonal compression strut was observed in the joint core. Therefore, NZS 3101 gave good prediction of joint shear strength with joint transverse reinforcement, as can be seen from the bold value of v_{j_max}/v_{jlimit} in Table 5. A shear strain of 1·1% implied that this specimen had undergone severe joint damage with wide cracks, as well as crushing and spalling of concrete, as depicted in Figure 8(a). Despite the fact that the maximum joint shear stress in specimen EIJ-S-0 is higher than that specified in NZS 3101 and ACI 318-14, no diagonal compression shear failure occurred in the joint. This suggests that the current joint shear stress limits specified by NZS 3101 and ACI 318-14 can be

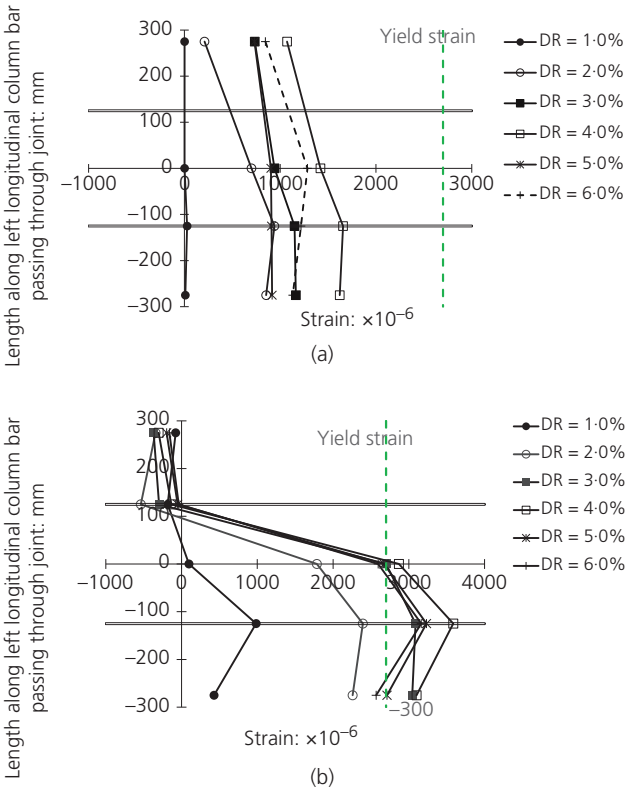

Figure 13. Distribution of strain along column left longitudinal bars passing through joint: (a) CIJ-NS-0; (b) EIJ-NS-0 (DR, drift ratio)

safely applied to ECC joints with no transverse reinforcement (Parra-Montesinos *et al.*, 2005).

Notably, allowable joint shear stress based on Eurocode 8 was overestimated for all specimens compared to the value given by NZS 3101 or ACI 318-14. This implied that Equations 4 through 7 in Eurocode 8 may not be conservative for predicting joint shear strength for columns without axial load. This is further supported by the value of $v_{j\_max}/v_{jlimit} = 0{\cdot}73$, as shown in Table 5 for CIJ-S-1, as this specimen failed in diagonal crushing of the joint.

Energy dissipation

Energy dissipation was computed from the summation of the area enclosed by each cycle of the hysteresis loops. For the purpose of comparison, the total cumulative energy dissipation at each cycle for each specimen was plotted up to 24 cycles (drift ratio of 6·0%), as shown in Figure 14. Obviously for non-seismic design, EIJ-NS-0 exhibited greater cumulative energy dissipation than CIJ-NS-0 (Figure 14(a)). This enhancement was about 76% during cycle number 24, despite the fact that EIJ-NS-0 experienced premature fracturing of rebars and had lower load capacity. For seismic design, the total energy dissipated in both specimens was similar (Figure 14(b)). This implies that EIJ-S-0 (with no transverse reinforcement in the joint) has comparable energy dissipation and performance with CIJ-S-1 (with transverse reinforcement in the joint). This clearly highlighted the effectiveness of ECC in resisting shear in the joint core. A similar observation was found in the test by Zhang *et al.* (2015), in which comparable energy dissipation was attained even after reducing the amount of transverse reinforcement in the beam and column regions of exterior beam–column sub-assemblages where ECC was used.

Conclusions

In this paper, experimental results of four RC beam–column sub-assemblages under cyclic loads were presented. The performance of ECC joints was evaluated for both seismic and non-seismic design scenarios and their behaviours were compared to specimens made of normal concrete joints with and without seismic design. The following conclusions can be drawn from the test results.

(*a*) Application of ECC in the joint of beam–column sub-assemblages (EIJ-NS-0 and EIJ-S-0) changed brittle shear failure in the joint to ductile flexural failure in the beam end region due to enhanced shear strain capacity in the ECC joint. This implies the possibility of relaxing the ratio of column flexural moment to beam flexural moment in Eurocode 8 to satisfy the strong-column–weak-beam design requirement. However, more tests should be conducted in future to substantiate this finding.

Table 5. Ratio of calculated maximum joint shear stress to limiting joint shear stress

Specimen	Compressive strength, f'_c: MPa	Calculated maximum joint shear stress, v_{j_max} according to Eurocode 8 by Equation 3: MPa	Calculated maximum joint shear stress v_{j_max} according to NZS 3101 and ACI 318-14 by Equation 3: MPa	Strain during v_{j_max}: %	Limiting joint shear stress v_{jlimit}: MPa (ratio v_{j_max}/v_{jlimit})		
					Eurocode 8 (Equation 4)	NZS ($0{\cdot}20\,f'_c$ or 10 MPa)	ACI 318-14 ($1{\cdot}25\sqrt{f'_c}$)
CIJ-NS-0	24·66	4·28	3·43	0·51	8·88 (0·48)	4·93 (0·70)	6·21 (0·55)
EIJ-NS-0	50·30	4·05	3·24	0·07	16·09 (0·25)	10·00 (0·32)	8·87 (0·37)
CIJ-S-1	24·66	6·51	5·21	1·10	8·88 (0·73)	**4·93 (1·06)**[a]	6·21 (0·84)
EIJ-S-0	50·30	7·86	6·29	0·38	16·09 (0·49)	10·00 (0·63)	8·87 (0·71)

[a]The value in bold indicates good prediction of joint shear strength with joint transverse reinforcement

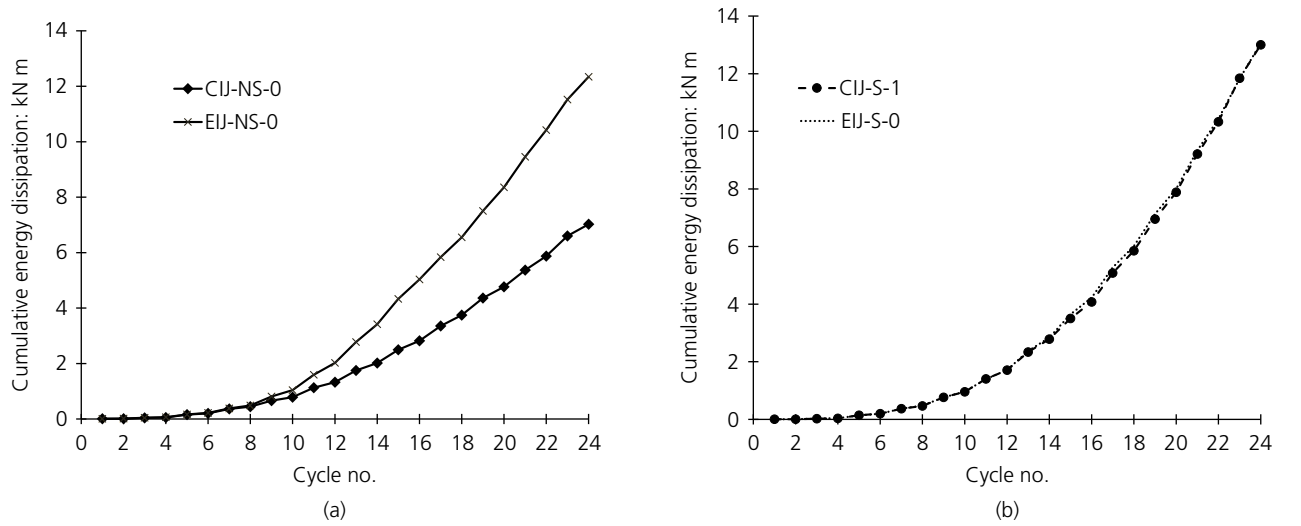

Figure 14. Cumulative energy dissipation: (a) non-seismic design; (b) seismic design

(*b*) The ECC was able to reduce shear distortion of joint cores owing to its multiple-cracking behaviour and superior ductility. Contribution of shear distortion to total drift was significantly decreased by 85–90% with the use of ECC in the joints compared to concrete joints at a drift ratio of 6·0%.

(*c*) Even though ECC specimens showed improved bond behaviour with beam longitudinal bars passing through the joint cores at the initial stage, bond deterioration occurred with widening of cracks at the joint interfaces as drift ratio increased. This was due to the presence of cold joints at the vertical joint interfaces.

(*d*) For beam–column sub-assemblages with non-seismic design, ECC improved total energy dissipation of EIJ-NS-0 by around 76% compared with CIJ-NS-0.

(*e*) Almost the same energy dissipation capacity was obtained for both specimens with seismic design (EIJ-S-0 and CIJ-S-1). However, ECC slightly increased the load capacity of the beam–column sub-assemblage by around 15%, despite the elimination of transverse reinforcement in the joint core of EIJ-S-0.

Acknowledgements

The authors would like to acknowledge the funding provided by the Protective Technology Research Centre in Nanyang Technological University, Singapore. Special acknowledgment is extended to Universiti Teknologi MARA, Malaysia for this research scholarship. The authors would like to thank Dr Kang Shao-Bo for his assistance in conducting the experimental works.

Appendix: Calculations on lateral displacement

Displacement Δ_{bf} due to flexural deformations of beams is given by

$$\Delta_{bf} = \delta_{bf}\frac{h}{l} \quad (8)$$

$$\delta_{bf} = \Sigma(\theta_{b,i})(l'_{b_i}) \quad (9)$$

$$\theta_{b,i} = \frac{\delta_{iT} - \delta_{iB}}{h_i} \quad (10)$$

where δ_{bf} represents the beam flexural deformations; h is the storey height of the column; l is the horizontal distance between the beam supports; $\theta_{b,i}$ is the rotation at section i (including fixed end); l'_{b_i} is the distance measured from section i to the centre of beam end support; δ_{iT} and δ_{iB} represent the readings of LVDTs mounted at the top and bottom faces of beam section i, respectively; h_i is the distance between the top and bottom LVDTs at section i. All details can be found in Figure 15.

Displacement Δ_{cf} due to flexural deformations of columns can be calculated from

$$\Delta_{cf} = \delta_{cf} \quad (11)$$

$$\delta_{cf} = \Sigma(\theta_{c,i})(l'_{c_i}) \quad (12)$$

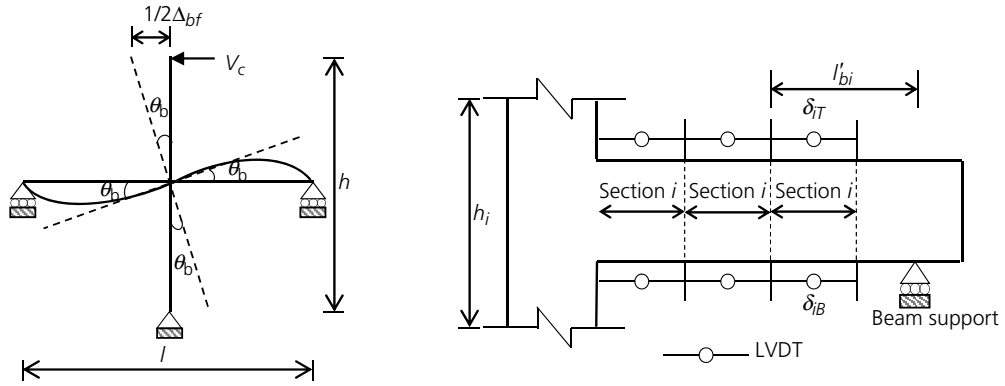

Figure 15. Determination of beam flexural deformations

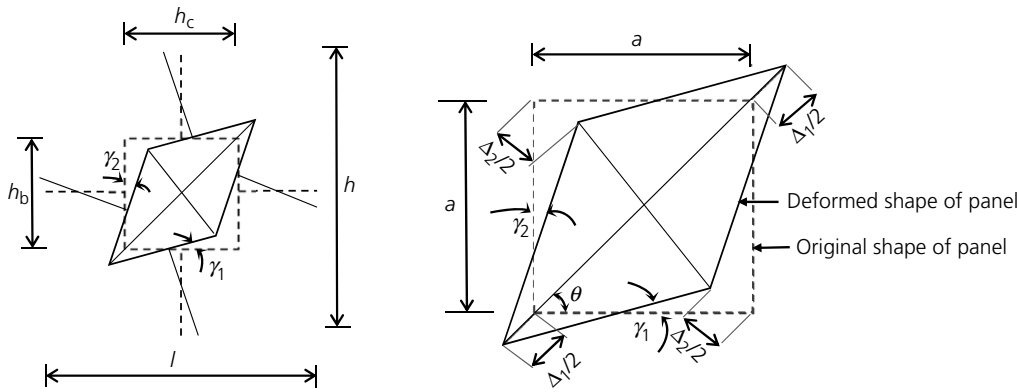

Figure 16. Determination of shear distortion at joint panel

13. $$\theta_{c,i} = \frac{\delta_{iR} - \delta_{iL}}{h_i'}$$

where δ_{cf} represents the column flexural deformations; $\theta_{c,i}$ is the rotation at section i (including fixed end); l_{c_i}' is the distance measured from section i to the centre of column end support; δ_{iR} and δ_{iL} represent the readings of LVDTs at the right and left faces of column section i, respectively; h_i' is the distance between the left and right LVDTs at section i. Displacement Δ_j contributed by shear distortion of the joint can be determined as

14. $$\Delta_j = \Upsilon_j\left(h - h_b - \frac{h}{l}h_c\right)$$

15. $$\Upsilon_j = \Upsilon_1 + \Upsilon_2 = \frac{\Delta_1 - \Delta_2}{\sqrt{2} \times a}$$

in which Υ_j represents the joint shear distortion; h_b and h_c are the depths of the beam and the column, respectively; Δ_1 and Δ_2 are the readings of diagonal LVDTs (S1 and S2) mounted on the joint; and a is taken as 200 mm, as shown in Figure 16.

REFERENCES

ACI (American Concrete Institute) (2015) Building code requirements for structural concrete (ACI 318-14). Commentary on building code requirements for structural concrete (ACI 318R-14). ACI, Farmington Hills, MI, USA.

Alyousif A, Anil O, Sahmaran M *et al.* (2015) Comparison of shear behaviour of engineered cementitious composite and normal concrete beams with different shear span lengths. *Magazine of Concrete Research* **68(5)**: 217–228, http://dx.doi.org/10.1680/jmacr.14.00336.

Ashtiani MS, Dhakal RP and Scott AN (2014) Seismic performance of high-strength self-compacting concrete in reinforced concrete beam–column joints. *Journal of Structural Engineering* **140(5)**: 04014002, https://doi.org/10.1061/(ASCE)ST.1943-541X.0000973.

BSI (2004a) BS EN 1998-1: Eurocode 8: Design of structures for earthquake resistance. BSI, London, UK.

BSI (2004b) BS EN 1992-1-1: Eurocode 2: Design of concrete structures: Part 1-1: general rules and rules for buildings. BSI, London, UK.

Fischer G and Li VC (2002) Effect of matrix ductility on deformation capacity behavior of steel-reinforced ECC flexural members under reversed cyclic loading conditions. *ACI Structural Journal* **99(6)**: 781–790.

Hakuto S (1995) *Retrofitting of Reinforced Concrete Moment Resisting Frames*. PhD thesis, University of Canterbury, Christchurch, New Zealand.

Hakuto S, Park R and Tanaka H (2000) Seismic load tests on interior and exterior beam–column joints with substandard reinforcing details. *Structural Journal* **97(1)**: 11–25.

Hossain KMA, Alam S, Anwar MS and Julkamine KMY (2017) Bond strength of fibre-reinforced polymer bars in engineered cementitious composites. *Proceedings of the Institution of Civil Engineers –Construction Materials*, in press, http://dx.doi.org/10.1680/jcoma.17.00020.

Kang SB, Tan KH and Yang EH (2015) Progressive collapse resistance of precast beam–column sub-assemblages with engineered cementitious composites. *Engineering Structures* **98**: 186–200, https://doi.org/10.1016/j.engstruct.2015.04.034.

Lee SW, Kang SB, Tan KH and Yang EH (2016) Experimental and analytical investigation on bond–slip behaviour of deformed bars embedded in engineered cementitious composites. *Construction and Building Materials* **127**: 494–503, https://doi.org/10.1016/j.conbuildmat.2016.10.036.

Li VC (2003) On engineered cementitious composites (ECC) a review of the material and its applications. *Journal of Advanced Concrete Technology* **1(3)**: 215–230.

Li VC and Fischer G (2002) Reinforced ECC – an evolution from materials to structures. *Proceedings of the 1st fib Congress, Osaka, Japan*. Citeseer, Osaka, Japan, pp. 105–102.

Li B, Lam ESS, Wu B and Wang YY (2015) Effect of high axial load on seismic behavior of reinforced concrete beam–column joints with and without strengthening. *ACI Structural Journal* **112(6)**: 713–723.

Parra-Montesinos GJ (2005) High-performance fiber-reinforced cement composites: an alternative for seismic design of structures. *ACI Structural Journal* **102(5)**: 668.

Parra-Montesinos GJ and Wight JK (2000) Seismic response of exterior RC column-to-steel beam connections. *Journal of Structural Engineering* **126(10)**: 1113–1121.

Parra-Montesinos GJ, Peterfreund SW and Chao SH (2005) Highly damage-tolerant beam–column joints through use of high-performance fiber-reinforced cement composites. *ACI Structural Journal* **102(3)**: 487–495.

Priestley MJN and Macrae GA (1996) Seismic tests of precast beam-to-column joint subassemblages with unbonded tendons. *PCI Journal* **41(1)**: 64–81.

Qudah S and Maalej M (2014) Application of engineered cementitious composites (ECC) in interior beam–column connections for enhanced seismic resistance. *Engineering Structures* **69**: 235–245, https://doi.org/10.1016/j.engstruct.2014.03.026.

Said SH and Razak HA (2016) Structural behavior of RC engineered cementitious composite (ECC) exterior beam–column joints under reversed cyclic loading. *Construction and Building Materials* **107**: 226–234, https://doi.org/10.1016/j.conbuildmat.2016.01.001.

SNZ (Standards New Zealand) (2006) NZS 3101.1: The design of concrete structures. Standards New Zealand, Wellington, New Zealand.

Tsonos AG (2007) Cyclic load behavior of reinforced concrete beam-column subassemblages of modern structures. *ACI Structural Journal* **104(4)**: 468.

Yuan F, Pan J, Xu Z and Leung CKY (2013) A comparison of engineered cementitious composites versus normal concrete in beam–column joints under reversed cyclic loading. *Materials and Structures* **46(1–2)**: 145–159.

Zhang R, Matsumoto K, Hirata T, Ishizeki Y and Niwa J (2015) Application of PP-ECC in beam–column joint connections of rigid-framed railway bridges to reduce transverse reinforcements. *Engineering Structures* **86**: 146–156, http://dx.doi.org/10.1016/j.engstruct.2015.01.005.

How can you contribute?

To discuss this paper, please submit up to 500 words to the editor at journals@ice.org.uk. Your contribution will be forwarded to the author(s) for a reply and, if considered appropriate by the editorial board, it will be published as a discussion in a future issue of the journal.